International Journal of Innovative
Computing, Information and Control
Volume **13**, Number **3**, June **2017**

ICIC International ©2017 ISSN 1349-4198
pp. 873–890

A CONTINUOUS FINITE-TIME ATTITUDE SYNCHRONIZATION APPROACH FOR SPACECRAFT FORMATIONS WITH COMMUNICATION DELAYS

Zhipeng Wang[1,*], Fengzhi Guo[1], Zhaowei Sun[1], Haichao Liang[2] and Jianying Wang[3]

[1]Research Center of Satellite Technology
Harbin Institute of Technology
No. 92, West Dazhi Street, Nangang District, Harbin 150001, P. R. China
*Corresponding author: wzp@hit.edu.cn

[2]Aeronautical and Astronautical Science and Technology
Beijing Institute of Space Long March Vehicle
Haidian District, Beijing 100000, P. R. China

[3]Science and Technology on Space Physics Laboratory
Haidian District, Beijing 100000, P. R. China

Received August 2016; revised January 2017

Abstract. *Synchronizing the attitude of formation flying spacecraft is an essential ingredient in almost all practical situations. However, thus far control schemes with finite-time convergent property have not been proposed for synchronizing the attitude of multiple spacecraft in the presence of communication delays. In this paper, a class of finite-time control schemes is developed to guarantee spacecraft attitude synchronization in the presence of communication delays, parameter uncertainties and external disturbances. Robustness, high tracking precision and finite-time convergence can be achieved simultaneously by the proposed control strategy despite the existence of these unexpected phenomena. The proposed control approach, which is based on an improved version of sliding mode control method, is continuous and so is chattering-free. Numerical simulations are provided to demonstrate the effectiveness of the proposed approach.*
Keywords: Attitude synchronization, Spacecraft formations, Finite-time control, Robustness, Communication delays

1. **Introduction.** Controlling the attitude of multiple autonomous vehicles in order to equalize their orientations is called attitude synchronization. Attitude synchronization of spacecraft formations has received an increasing interest in the field of aerospace technology. This interest is motivated by their applications in synthetic-aperture imaging and space-based interferometry, and their potential advantages such as cost reduction and reliability improvement [1-4].

Recent results in this area are generally inspired by the virtual structure method [5], behavior-based approach [6,7], variable structure control strategy [8], energy shaping algorithm [9], adaptive control method [10,11], and so on [12-15]. These works aimed to design control schemes for a swarm of spacecraft based on local information transmission to achieve a common control objective. For instance, behavior-based control was adopted in [6,7] to solve the attitude coordination problem of spacecraft formations. The basic idea of behavior-based control is to determine the control action by a weighted sum of each behavior. On the basis of variable structure control method, attitude synchronization of spacecraft formations with communication delays was investigated in [8]. Both the disturbance torques and parameter uncertainties were taken into account in controller design

but only the attitude regulation problem was addressed and the control laws were discontinuous due to the sign function. Spacecraft formations with directed communication topologies were investigated in [10]. In the presence of uncertainties, system's robustness was improved by means of adaptive control method. In particular, the authors in [12] solved the attitude containment control problem by the use of finite-time control approach. By considering the existence of multiple leaders, the attitude states of the followers were able to converge to the convex hull of the leaders' orientations. However, the effects of external disturbances and model uncertainties were not investigated.

In spite of the interesting results cited above, much work remains to be done to develop control schemes for spacecraft formations in the presence of communication delays, parameter uncertainties and external disturbances.

In practical situations, SFF is challenging since the information is always transmitted and exchanged through a wireless network, and the communication is far from being perfect. A critical issue is that the information transmission between spacecraft is usually delayed. In the field of first and second order dynamics systems, synchronization with communication delays was studied, and sufficient conditions have been derived to obtain stability of the system [16-18]. Nevertheless, few works have been done for nonlinear formation system, especially spacecraft formation systems. Synchronization of bilateral teleoperators was investigated in [19] by means of passivity-based control. Lagrange formulation of spacecraft dynamics was utilized in [20] and the authors solved the spacecraft formation control problem. Another problem of the communication network is that the undirected communication topology considered in [4-8,11-15] is an assumption that needs to be checked all the time. The topology in practical flying missions can be various types rather than undirected such as unidirectional satellite laser communication system [10].

In addition to the aforementioned issue, parameter uncertainty always exists in practical situation due to the unmodelled dynamics, fuel consumption and uncertain center of mass position. Moreover, external disturbance is also an ineluctable problem induced by environmental factors such as gravity gradient, aerodynamics, and solar radiation. Ignoring parameter uncertainties and environmental torques can jeopardize the mission. An effective tool to solve this problem is finite time control approach which has been extensively studied in recent decades, since finite-time stabilization of dynamical systems may give rise to a high-precision control performance and robustness against uncertainties and disturbances besides the finite-time convergent property.

Finite-time stability and convergence can be obtained by continuous feedback control schemes [12], but the robustness of such type of controllers has not been fully investigated. Another method is the terminal sliding mode (TSM) control which has been studied and applied in single-rigid-body systems [21-26]. The regulation problem of robotic manipulators was investigated in [22]. The authors in [25] realized the finite-time tracking of a single robotic manipulator using terminal sliding mode technique. Thus far, finite-time control based on TSM has been little utilized in formation systems. In addition, TSM control is discontinuous so that chattering exists in the generated control signals. Chattering phenomenon, as well-known, is harmful for any mechanical system. Therefore, designing continuous TSM control schemes with robustness against uncertainties and disturbances is desirable.

Inspired by these facts, it is interesting and challenging to solve the attitude synchronization problem of spacecraft formations with communication delays, parameter uncertainties and environmental disturbances by means of a continuous finite-time control approach. To the best of the author's knowledge, such type of control problem has not been addressed in the existing literature.

In this paper, we focus on the design of continuous finite-time attitude synchronization controllers for spacecraft formations subject to communication delays, parameter uncertainties and external disturbances. This scenario is important to practical applications such as reorientation, attitude tracking, and observation of moving objectives. Based on TSM control strategy, a class of continuous attitude synchronization control algorithms is developed to guarantee finite-time reachability of the desired attitude and to keep certain relative attitude between spacecraft within the formation. Finite-time convergence and high control precision of the proposed control schemes in the presence of these unexpected phenomena is proven mathematically.

The rest of this paper is organized as follows. In Section 2, preliminaries are given. In Section 3, continuous control schemes with finite-time convergent property are proposed, and discussions on robustness of the proposed control algorithm are provided. In Section 4, numerical simulations demonstrating the effectiveness of the control schemes are presented. Finally, Section 5 concludes this paper.

Notations

Given a vector $\boldsymbol{\Lambda}$, $\boldsymbol{\Lambda}_i$ is used to denote parameter or variable of the i-th spacecraft within the formation, where $i = 1, 2, \ldots, n$ and $\boldsymbol{\Lambda}_{(k)}$ is used to represent the k-th component of the vector $\boldsymbol{\Lambda}$.

2. **Preliminaries.** In this section, three coordinate frames are defined. $\mathbf{I}$ is the inertial reference frame. $\mathbf{B}$ is the body fixed reference frame, where origin locates at the centroid of the spacecraft, and the axes coincide with its principal axis of inertia. $\mathbf{D}$ is a desired reference frame whose origin locates at the centroid of the spacecraft and the three axes point to the desired orientation.

The modified Rodrigues parameters (MRPs) [27] are adopted herein for the description of a rigid spacecraft's attitude. The definition of the MRPs is

$$\boldsymbol{\sigma} = \boldsymbol{n} \cdot \tan(\theta/4) \tag{1}$$

where $\boldsymbol{n}$ denotes the Euler axis with the Euler principal angle represented by θ. The MRPs representation is a three-dimensional attitude description with no sign ambiguity and it can represent the attitude state without any singularity in $\theta \in (-360, +360)$ deg.

We use $\boldsymbol{\sigma} \in R^3$ to represent the absolute attitude state of $\mathbf{B}$ with respect to $\mathbf{I}$. The absolute angular velocity $\boldsymbol{\omega} \in R^3$ represents the angular velocity of $\mathbf{B}$ with respect to $\mathbf{I}$ expressed in $\mathbf{B}$.

The kinematics equation is defined as follows

$$\dot{\boldsymbol{\sigma}} = \boldsymbol{G}(\boldsymbol{\sigma})\,\boldsymbol{\omega} \tag{2}$$

where

$$\boldsymbol{G}(\boldsymbol{\sigma}) = \frac{1}{4}\left\{\left(1 - \boldsymbol{\sigma}^T\boldsymbol{\sigma}\right)\boldsymbol{I} + 2\left[\boldsymbol{\sigma}^{\times}\right] + 2\boldsymbol{\sigma}\boldsymbol{\sigma}^T\right\} \tag{3}$$

$\boldsymbol{I}$ denotes a 3×3 identity matrix and $\boldsymbol{\sigma}^{\times}$ is a skew-symmetric matrix defined as

$$\boldsymbol{\sigma}^{\times} = \begin{bmatrix} 0 & -\boldsymbol{\sigma}_{(3)} & \boldsymbol{\sigma}_{(2)} \\ \boldsymbol{\sigma}_{(3)} & 0 & -\boldsymbol{\sigma}_{(1)} \\ -\boldsymbol{\sigma}_{(2)} & \boldsymbol{\sigma}_{(1)} & 0 \end{bmatrix} \tag{4}$$

The absolute attitude error $\boldsymbol{\sigma}_e \in R^3$ defined by

$$\boldsymbol{\sigma}_e = \boldsymbol{\sigma} \otimes (-\boldsymbol{\sigma}_d) = \frac{\boldsymbol{\sigma}_d\left(\boldsymbol{\sigma}^T\boldsymbol{\sigma} - 1\right) + \boldsymbol{\sigma}\left(1 - \boldsymbol{\sigma}_d^T\boldsymbol{\sigma}_d\right) - 2\boldsymbol{\sigma}_d^{\times}\boldsymbol{\sigma}}{1 + \boldsymbol{\sigma}_d^T\boldsymbol{\sigma}_d\boldsymbol{\sigma}^T\boldsymbol{\sigma} + 2\boldsymbol{\sigma}_d^T\boldsymbol{\sigma}} \tag{5}$$

is the orientation from $\mathbf{D}$ to $\mathbf{B}$, where symbol $\otimes$ represents the MRPs multiplication, $\boldsymbol{\sigma}_d$ is the orientation from $\mathbf{I}$ to $\mathbf{D}$. According to Equation (2), we have $\dot{\boldsymbol{\sigma}}_e = \boldsymbol{G}_e\boldsymbol{\omega}_e$ where $\boldsymbol{G}_e = \boldsymbol{G}(\boldsymbol{\sigma}_e)$. $\boldsymbol{\omega}_e \in R^3$ is the absolute angular velocity error. $\boldsymbol{\omega}_e$ can be calculated using

$$\boldsymbol{\omega}_e = \boldsymbol{\omega} - \boldsymbol{M}_e\boldsymbol{\omega}_d \tag{6}$$

where $\boldsymbol{\omega}_d \in R^3$ is the desired angular velocity which should be sufficiently smooth and the derivative of which should be bounded, and $\boldsymbol{M}_e \in R^{3\times 3}$ denotes the rotation matrix from $\mathbf{D}$ to $\mathbf{B}$, which can be calculated using

$$\boldsymbol{M}_e = \boldsymbol{I}_3 - \frac{4\left(1-\boldsymbol{\sigma}_e^2\right)}{\left(1+\boldsymbol{\sigma}_e^2\right)^2}\left[\boldsymbol{\sigma}_e^{\times}\right] + \frac{8}{\left(1+\boldsymbol{\sigma}_e^2\right)^2}\left[\boldsymbol{\sigma}_e^{\times}\right]^2 \tag{7}$$

The dynamics of a rigid satellite can be written as

$$\boldsymbol{J}\dot{\boldsymbol{\omega}} = -\boldsymbol{\omega}^{\times}\boldsymbol{J}\boldsymbol{\omega} + \boldsymbol{u} \tag{8}$$

where $\boldsymbol{J} \in R^{3\times 3}$ represents the inertia tensor of the spacecraft, $\boldsymbol{u} \in R^3$ is the control torque. According to Equation (6), the dynamic model representing the relative angular rate can be stated as

$$\boldsymbol{J}\dot{\boldsymbol{\omega}}_e = -\boldsymbol{\omega}^{\times}\boldsymbol{J}\boldsymbol{\omega} + \boldsymbol{u} - \boldsymbol{J}\left(\boldsymbol{M}_e\dot{\boldsymbol{\omega}}_d - \boldsymbol{\omega}_e^{\times}\boldsymbol{M}_e\boldsymbol{\omega}_d\right) = \boldsymbol{W} + \boldsymbol{u} \tag{9}$$

where $\boldsymbol{W} = -\boldsymbol{\omega}^{\times}\boldsymbol{J}\boldsymbol{\omega} - \boldsymbol{J}\left(\boldsymbol{M}_e\dot{\boldsymbol{\omega}}_d - \boldsymbol{\omega}_e^{\times}\boldsymbol{M}_e\boldsymbol{\omega}_d\right)$.

In order to facilitate the stability and convergence analysis, the following lemma is presented.

Lemma 2.1. [28] *A function $V(x)$ is positive definite and homogeneous of degree σ to the dilation $(r_1, \ldots, r_n)$. If $\widetilde{V}(x)$ is a continuous function such that, for any fixed $x \neq 0$, $\frac{\widetilde{V}\left(\rho^{r_1}x_1,\ldots,\rho^{r_n}x_n\right)}{\rho^{\sigma}} \to 0$ as $\rho \to 0$, then $V + \widetilde{V}$ is locally positive definite.*

3. Controllers Design.

3.1. Problem statement.

An n-spacecraft formation performing a flying task in which the spacecraft within the formation is required to align their attitudes while tracking a time-varying reference state $\{\boldsymbol{\sigma}_d(t), \boldsymbol{\omega}_d(t)\}$ is considered in this study. The attitude control problem herein is to design continuous finite-time control schemes for a spacecraft formation by the use of the behavior-based control approach, such that the attitude of each spacecraft can converge to the reference state in finite time and maintain certain relative attitude with arbitrary communication topologies in the presence of time delays, model uncertainties and external disturbances.

3.2. Fast sliding mode.

In this subsection, a fast sliding mode (FSM) is proposed to guarantee finite-time reachability of the equilibrium. The FSM is given as follows:

$$\boldsymbol{s}_i = \boldsymbol{\omega}_{ei} + a\boldsymbol{\sigma}_{ei} + b\mathrm{sig}\left(\boldsymbol{\sigma}_{ei}\right)^{\frac{p}{q}} \tag{10}$$

where $\mathrm{sig}\left(\boldsymbol{\sigma}_{ei}\right)^{\frac{p}{q}} = sgn\left(\boldsymbol{\sigma}_{ei}\right)\left|\boldsymbol{\sigma}_{ei}\right|^{\frac{p}{q}}$; a and b are positive constants; p and q which are used to represent the fractional power are positive odd numbers satisfying $\frac{1}{2} < \frac{p}{q} < 1$.

Theorem 3.1. *The equilibrium point $(\boldsymbol{\sigma}_{ei} = 0, \boldsymbol{\omega}_{ei} = 0)$ of the differential Equation (10) is finite-time stable: the system states $(\boldsymbol{\sigma}_{ei}, \boldsymbol{\omega}_{ei})$ reaching the sliding mode $\boldsymbol{s}_i \equiv 0$ will converge to the equilibrium point in finite time T and stay there forever such that $(\boldsymbol{\sigma}_{ei} = 0$, $\boldsymbol{\omega}_{ei} = 0)$ for $t > T$.*

Proof: Consider the following positive scalar function:

$$V_i = 2\ln\left(1+\boldsymbol{\sigma}_{ei}^T\boldsymbol{\sigma}_{ei}\right) \tag{11}$$

Calculating the first-order derivative of V_i yields

$$\dot{V}_i = \frac{4\boldsymbol{\sigma}_{ei}^T\dot{\boldsymbol{\sigma}}_{ei}}{1+\boldsymbol{\sigma}_{ei}^T\boldsymbol{\sigma}_{ei}} = \frac{4\boldsymbol{\sigma}_{ei}^T\boldsymbol{G}_{ei}\boldsymbol{\omega}_{ei}}{1+\boldsymbol{\sigma}_{ei}^T\boldsymbol{\sigma}_{ei}} = \boldsymbol{\sigma}_{ei}^T\boldsymbol{\omega}_{ei} \tag{12}$$

Since

$$\boldsymbol{\omega}_{ei} = -a\boldsymbol{\sigma}_{ei} - b\mathrm{sig}\left(\boldsymbol{\sigma}_{ei}\right)^{\frac{p}{q}} \tag{13}$$

when $\boldsymbol{s}_i \equiv 0$, it follows that

$$\dot{V}_i = \boldsymbol{\sigma}_{ei}^T\left(-a\boldsymbol{\sigma}_{ei} - b\mathrm{sig}\left(\boldsymbol{\sigma}_{ei}\right)^{\frac{p}{q}}\right) = -a\boldsymbol{\sigma}_{ei}^T\boldsymbol{\sigma}_{ei} - b\left|\boldsymbol{\sigma}_{ei}\right|^{\frac{p+q}{q}} \le -c_1V_i - c_2V_i^{\frac{p+q}{2q}} \tag{14}$$

where $c_1 = \frac{a}{2}$ and $c_2 = 2^{-\frac{p+q}{2q}}b$. By integrating the both sides of (14), it can be derived that

$$\int_0^T -dt \ge \int_{V_i(0)}^0 \frac{dV_i}{-c_1V_i - c_2V_i^{\frac{p+q}{2q}}} \qquad T \le \frac{q}{c_1(q-p)}\ln\left(\frac{c_1\left|V_i(0)\right|^{\frac{q-p}{q}}+c_2}{c_2}\right) \tag{15}$$

where $V_i(0)$ represents the initial value of V_i. Therefore, it is proven that $V_i = 0$ can be achieved in finite time, and thus $\boldsymbol{\sigma}_{ei} = 0$ and $\boldsymbol{\omega}_{ei} = 0$ according to (13) can be obtained in finite time. This completes the proof.

The proposed FSM is a combination of the linear-hyperplane sliding mode (LSM) and the terminal sliding mode (TSM). When the system state $\boldsymbol{\sigma}_{ei}$ is far away from the origin, the linear part $-c_1\boldsymbol{\sigma}_{ei}$ prevails over its counterpart $-c_2\mathrm{sig}\left(\boldsymbol{\sigma}_{ei}\right)^{\alpha}$ such that the convergence rate depends on the linear part $-c_1\boldsymbol{\sigma}_{ei}$: the fast convergence rate when the system states are far away from the origin is well understood. When the system state is close to the origin, then the convergence rate mainly depends on the terminal part $-c_2\mathrm{sig}\left(\boldsymbol{\sigma}_{ei}\right)^{\alpha}$: it makes the control objective be achieved in finite time since the convergence rate accelerates exponentially as the states approach the equilibrium.

3.3. **Synchronization controllers.** There are two objectives when synchronizing the attitude of the spacecraft formation: station keeping (desired attitude attainment) and formation keeping (relative attitude maintenance). A tool that is effective to deal with the existence of multiple control objectives is the behavior-based approach adopted in [6,7]. Based on the behavior-based control algorithm, the following attitude synchronization control schemes are proposed:

$$\boldsymbol{u}_i = \boldsymbol{u}_{is} + \boldsymbol{u}_{if}, \quad i = 1, 2, \ldots, n \tag{16}$$

where $\boldsymbol{u}_i$ is the control law for the i-th spacecraft within the formation, and

$$\boldsymbol{u}_{is} = -\boldsymbol{W}_i - \boldsymbol{J}_i\boldsymbol{Q}_i - \gamma_i\mathrm{sig}(\boldsymbol{s}_i)^{\frac{p}{q}} \tag{17}$$

$$\boldsymbol{u}_{if} = -\sum_{j=1}^{n} k_i\left(\mathrm{sig}\left(\boldsymbol{s}_i\right)^{\frac{r}{q}} - \delta_{ij}\mathrm{sig}\left(\boldsymbol{s}_j\left(\tau_{ij}\right)\right)^{\frac{r}{q}}\right) \tag{18}$$

are the control actions for station keeping and formation keeping, respectively, where γ_i is a positive constant; $\boldsymbol{Q}_i \in R^3 = a\dot{\boldsymbol{\sigma}}_{ei} + \frac{bp}{q}\left|\boldsymbol{\sigma}_{ei}\right|^{\frac{p-q}{q}}\dot{\boldsymbol{\sigma}}_{ei}$; $\boldsymbol{s}_i$ is the FSM; r is a positive odd number satisfying $p < r < q$; $\delta_{ij} = 0, 1$ is a binary value describing the communication link between the i-th and j-th spacecraft; k_i is a positive weight parameter for the formation-keeping control action, the value of which can affect the closed-loop performance of the spacecraft formation.

The control schemes are designed by the use of the behavior-based control method. $\boldsymbol{u}_{is}$ is the station-keeping control term to drive the i-th spacecraft to the desired state, and $\boldsymbol{u}_{if}$ is the formation-keeping control term to keep the relative attitude control accuracy. The control law $\boldsymbol{u}_i$ is designed by a weighted sum of the two control terms.

Theorem 3.2. *The proposed controller (10) can solve the attitude synchronization problem of spacecraft formations with communication delays subject to arbitrary communication topologies, if $k_i > \beta$ and $(k_i)^2 \leq 4(k_i - \beta)$ hold, where β is a positive constant that will be involved in the stability and convergence analysis.*

Proof: Consider the following positive scalar function:

$$\begin{aligned}\widehat{V} = V + \underset{\sim}{V} = &\frac{q}{(r+q)} \sum_{i=1}^{n} \operatorname{sig}(\boldsymbol{s}_i)^{\frac{r+q}{2q}T} \boldsymbol{J}_i \operatorname{sig}(\boldsymbol{s}_i)^{\frac{r+q}{2q}} \\ &+ \beta \sum_{i=1}^{n} \sum_{j=1}^{n} \int_{t-\tau_{ij}}^{t} \operatorname{sig}(\boldsymbol{s}_j)^{\frac{r}{q}T} \operatorname{sig}(\boldsymbol{s}_j)^{\frac{r}{q}} dx\end{aligned} \tag{19}$$

It can be seen that V is positive definite. Computing the derivative of V, we have

$$\begin{aligned}\dot{V} = &\frac{q}{(r+q)} \sum_{i=1}^{n} \operatorname{sig}(\boldsymbol{s}_i)^{\frac{r+q}{2q}T} \boldsymbol{J}_i \left[\frac{r+q}{2q} \operatorname{diag}\left(|\boldsymbol{s}_i|^{\frac{r-q}{2q}}\right) \dot{\boldsymbol{s}}_i\right] \\ &+ \frac{q}{(r+q)} \sum_{i=1}^{n} \left[\frac{r+q}{2q} \operatorname{diag}\left(|\boldsymbol{s}_i|^{\frac{r-q}{2q}}\right) \dot{\boldsymbol{s}}_i\right]^T \boldsymbol{J}_i \operatorname{sig}(\boldsymbol{s}_i)^{\frac{r+q}{2q}} \\ = &\sum_{i=1}^{n} \operatorname{sig}(\boldsymbol{s}_i)^{\frac{r}{q}T} \left(\boldsymbol{J}_i \dot{\boldsymbol{\omega}}_{ei} + \boldsymbol{J}_i \left[a\dot{\boldsymbol{\sigma}}_{ei} + \frac{bp}{q} |\boldsymbol{\sigma}_{ei}|^{\frac{p-q}{q}} \dot{\boldsymbol{\sigma}}_{ei}\right]\right) \\ = &\sum_{i=1}^{n} \operatorname{sig}(\boldsymbol{s}_i)^{\frac{r}{q}T} \left(\boldsymbol{J}_i \dot{\boldsymbol{\omega}}_{ei} + \boldsymbol{J}_i \boldsymbol{Q}_i\right)\end{aligned} \tag{20}$$

Substituting the relative dynamics Equations (9) into (20) yields

$$\begin{aligned}\dot{V} = &\sum_{i=1}^{n} \operatorname{sig}(\boldsymbol{s}_i)^{\frac{r}{q}T} \left(\boldsymbol{W}_i + \boldsymbol{u}_i + \boldsymbol{J}_i \boldsymbol{Q}_i\right) \\ = &\sum_{i=1}^{n} \operatorname{sig}(\boldsymbol{s}_i)^{\frac{r}{q}T} \left(-\gamma_i \operatorname{sig}(\boldsymbol{s}_i)^{\frac{p}{q}} + \boldsymbol{u}_{if}\right) \\ = &\sum_{i=1}^{n} \left\{-\gamma_i \operatorname{sig}(\boldsymbol{s}_i)^{\frac{r}{q}T} \operatorname{sig}(\boldsymbol{s}_i)^{\frac{p}{q}} - \operatorname{sig}(\boldsymbol{s}_i)^{\frac{r}{q}T} \sum_{j=1}^{n} k_i \left(\operatorname{sig}(\boldsymbol{s}_i)^{\frac{r}{q}T}\right.\right. \\ &\left.\left. - \delta_{ij} \operatorname{sig}(\boldsymbol{s}_j(\tau_{ij}))^{\frac{r}{q}T}\right)\right\}\end{aligned} \tag{21}$$

Next, calculating the first-order derivative of $\underset{\sim}{V}$ yields

$$\dot{\underset{\sim}{V}} = \beta \sum_{i=1}^{n} \sum_{j=1}^{n} \left[\operatorname{sig}(\boldsymbol{s}_i)^{\frac{r}{q}T} \operatorname{sig}(\boldsymbol{s}_i)^{\frac{r}{q}} - \operatorname{sig}(\boldsymbol{s}_j(\tau_{ij}))^{\frac{r}{q}T} \operatorname{sig}(\boldsymbol{s}_j(\tau_{ij}))^{\frac{r}{q}}\right] \tag{22}$$

Then $\dot{\widehat{V}}$ can be calculated as

$$\begin{aligned}
\dot{\widehat{V}} =& \dot{V} + \dot{\underset{\sim}{V}} \\
=& -\sum_{i=1}^{n} \gamma_i \mathrm{sig}\left(\boldsymbol{s}_i\right)^{\frac{r}{q}T} \mathrm{sig}\left(\boldsymbol{s}_i\right)^{\frac{p}{q}} - \sum_{i=1}^{n} \mathrm{sig}\left(\boldsymbol{s}_i\right)^{\frac{r}{q}T} \sum_{j=1}^{n} k_i \left[\mathrm{sig}\left(\boldsymbol{s}_i\right)^{\frac{r}{q}} - \delta_{ij} \mathrm{sig}\left(\boldsymbol{s}_j\left(\tau_{ij}\right)\right)^{\frac{r}{q}}\right] \\
&+ \beta \sum_{i=1}^{n}\sum_{j=1}^{n} \left[\mathrm{sig}\left(\boldsymbol{s}_i\right)^{\frac{r}{q}T} \mathrm{sig}\left(\boldsymbol{s}_i\right)^{\frac{r}{q}} - \mathrm{sig}\left(\boldsymbol{s}_j\left(\tau_{ij}\right)\right)^{\frac{r}{q}T} \mathrm{sig}\left(\boldsymbol{s}_j\left(\tau_{ij}\right)\right)^{\frac{r}{q}}\right] \\
=& -\sum_{k=1}^{3}\sum_{i=1}^{n} \gamma_i \left(\mathrm{sig}\left(\boldsymbol{s}_i\right)^{\frac{r+p}{q}}\right)_k - \beta \sum_{i=1}^{n}\sum_{j=1}^{n} \mathrm{sig}\left(\boldsymbol{s}_j\left(\tau_{ij}\right)\right)^{\frac{r}{q}T} \mathrm{sig}(\boldsymbol{s}_j(\tau_{ij}))^{\frac{r}{q}} \\
&- \sum_{i=1}^{n}\sum_{j=1}^{n} \left\{\left(k_i - \beta\right) \mathrm{sig}\left(\boldsymbol{s}_i\right)^{\frac{r}{q}T} \mathrm{sig}\left(\boldsymbol{s}_i\right)^{\frac{r}{q}} - \delta_{ij} k_i \mathrm{sig}\left(\boldsymbol{s}_i\right)^{\frac{r}{q}T} \mathrm{sig}\left(\boldsymbol{s}_j\left(\tau_{ij}\right)\right)^{\frac{r}{q}}\right\} \\
=& -\sum_{k=1}^{3}\sum_{i=1}^{n} \gamma_i \left(\mathrm{sig}\left(\boldsymbol{s}_i\right)^{\frac{r+p}{q}}\right)_k - \sum_{i=1}^{n}\sum_{j=1}^{n} \boldsymbol{\Psi}_{ij}^T \boldsymbol{\Psi}_{ij} \\
&- \sum_{i=1}^{n}\sum_{j=1}^{n} \left[1 - \frac{\left(\delta_{ij} k_i\right)^2}{4\left(k_i - \beta\right)}\right] \left(\boldsymbol{s}_j\left(\tau_{ij}\right)\right)^{\frac{r}{q}T} \mathrm{sig}\left(\boldsymbol{s}_j\left(\tau_{ij}\right)^{\frac{r}{q}}\right) \\
\leq& -\sum_{k=1}^{3}\sum_{i=1}^{n} \gamma_i \left(\mathrm{sig}\left(\boldsymbol{s}_i\right)^{\frac{r+p}{q}}\right)_k
\end{aligned} \tag{23}$$

with $\boldsymbol{\Psi}_{ij} = \sqrt{k_i - \beta}\mathrm{sig}\left(\boldsymbol{s}_i\right)^{\frac{r}{q}} - \delta_{ij}\frac{k_i}{2\sqrt{k_i - \beta}}\mathrm{sig}\left(\boldsymbol{s}_j\left(\tau_{ij}\right)\right)^{\frac{r}{q}}$. Then, it can be derived that

$$\begin{aligned}
\dot{V} \leq& -\sum_{k=1}^{3}\sum_{i=1}^{n} \gamma_i \left(\mathrm{sig}\left(\boldsymbol{s}_i\right)^{\frac{p+r}{q}}\right)_k - \dot{\underset{\sim}{V}} \\
=& -\frac{1}{2}\sum_{k=1}^{3}\sum_{i=1}^{n} \gamma_i \left(\mathrm{sig}\left(\boldsymbol{s}_i\right)^{\frac{p+r}{q}}\right)_k - \left\{\frac{1}{2}\sum_{k=1}^{3}\sum_{i=1}^{n} \gamma_i \left(\mathrm{sig}\left(\boldsymbol{s}_i\right)^{\frac{p+r}{q}}\right)_k \right. \\
&\left. + \beta \sum_{i=1}^{n}\sum_{j=1}^{n} \left[\mathrm{sig}\left(\boldsymbol{s}_i\right)^{\frac{r}{q}T} \mathrm{sig}\left(\boldsymbol{s}_i\right)^{\frac{r}{q}} - \mathrm{sig}\left(\boldsymbol{s}_j\left(\tau_{ij}\right)\right)^{\frac{r}{q}T} \mathrm{sig}\left(\boldsymbol{s}_j\left(\tau_{ij}\right)\right)^{\frac{r}{q}}\right]\right\}
\end{aligned} \tag{24}$$

According to Lemma 2.1, the term

$$\begin{aligned}
&\frac{1}{2}\sum_{k=1}^{3}\sum_{i=1}^{n} \gamma_i \left(\mathrm{sig}\left(\boldsymbol{s}_i\right)^{\frac{p+r}{q}}\right)_k \\
&+ \beta \sum_{i=1}^{n}\sum_{j=1}^{n} \left[\mathrm{sig}\left(\boldsymbol{s}_i\right)^{\frac{r}{q}T} \mathrm{sig}\left(\boldsymbol{s}_i\right)^{\frac{r}{q}} - \mathrm{sig}\left(\boldsymbol{s}_j\left(\tau_{ij}\right)\right)^{\frac{r}{q}T} \mathrm{sig}\left(\boldsymbol{s}_j\left(\tau_{ij}\right)\right)^{\frac{r}{q}}\right]
\end{aligned} \tag{25}$$

is locally positive definite since $p < r < q$. Then, it can be derived from (24) that

$$\dot{V} \leq -\frac{1}{2}\sum_{k=1}^{3}\sum_{i=1}^{n} \gamma_i \left(\mathrm{sig}\left(\boldsymbol{s}_i\right)^{\frac{p+r}{q}}\right)_k \leq -\varepsilon V^{\frac{p+r}{2q}} \tag{26}$$

where $\varepsilon = \left\{\frac{2}{\min[\alpha_{\min}(\boldsymbol{J}_i)]}\right\}^{\frac{p+r}{2p}} \frac{\max(\gamma_i)}{2}$ for $i = 1, \ldots, n$. By integrating both sides of (20), it gives that

$$\int_0^T -dt \geq \int_{V(0)}^0 \frac{dV}{\varepsilon V^{\frac{p+r}{2q}}} \qquad T \leq \frac{2q}{\varepsilon(2q-p-r)} |V(0)|^{\frac{2q-p-r}{2q}} \tag{27}$$

where $V(0)$ represents the initial value of V.

Therefore, $V = 0$ is proven to be achieved in finite time, and it follows that $\boldsymbol{s}_i = 0$ for $i = 1, \ldots, n$ is achieved in finite time. According to Theorem 3.1, it is safe to conclude that the control objective ($\boldsymbol{\sigma}_{ei} = 0, \boldsymbol{\omega}_{ei} = 0$) is obtained in finite time. This completes the proof.

3.4. **Robustness discussion.** One ineluctable problem for any SFF is the parameter uncertainties since the moments of inertia vary with fuel consumption and uncertain center of mass position. Another problem is the existence of environmental disturbances. Ignoring uncertainties and environmental disturbing torques can jeopardize the mission. In this section, we consider the parameter uncertainties and disturbance torque in the dynamics equation to analyze the performance of the proposed control strategies. If we use $\boldsymbol{d} \in R^3$ to represent the external disturbances and $\overline{\boldsymbol{J}}_i$, $\boldsymbol{J}_i$ and $\Delta\boldsymbol{J}_i$ satisfying $\overline{\boldsymbol{J}}_i = \boldsymbol{J}_i + \Delta\boldsymbol{J}_i$ to represent the real inertia tensor, nominal inertia tensor and uncertain inertia tensor, respectively, then the dynamic model of the spacecraft can be restated as

$$\boldsymbol{J}\dot{\omega}_e = \boldsymbol{W} + \boldsymbol{u} + \boldsymbol{d} + \Delta\boldsymbol{W} \tag{28}$$

where $\Delta\boldsymbol{W} = -\boldsymbol{\omega}\times\Delta\boldsymbol{J}\boldsymbol{\omega} - \Delta\boldsymbol{J}\left(\boldsymbol{M}_e\dot{\boldsymbol{\omega}}_d - \boldsymbol{\omega}_e \times \boldsymbol{M}_e\boldsymbol{\omega}_d\right)$ denotes the uncertain term induced by unmodelled dynamics.

Corollary 3.1. *In the presence of uncertainties and disturbance torques, the proposed control algorithms (10) steer the attitude of each spacecraft to a neighborhood of the sliding mode $\boldsymbol{s}_i = 0$ as*

$$\|\boldsymbol{s}_i\| \leq \Phi_i = \left(\frac{\tilde{\Phi}_i}{\gamma_i}\right)^{\frac{q}{p}} \tag{29}$$

in finite time where $\tilde{\Phi}_i = \|\boldsymbol{d}_i + \Delta\boldsymbol{W}_i + \Delta\boldsymbol{Q}_i\|$ with $\Delta\boldsymbol{Q}_i = \Delta\boldsymbol{J}_i\boldsymbol{Q}_i$. Furthermore, the tracking errors converge to a neighborhood of the equilibrium as

$$|(\boldsymbol{\sigma}_{ei})_k| \leq \min\left[\frac{\Phi_i}{a}, \left(\frac{\Phi_i}{b}\right)^{\frac{q}{p}}\right], \quad k = 1, 2, 3 \tag{30}$$

in finite time.

Proof: We still consider the Lyapunov Function (13). It is derived that

$$\dot{V} = \sum_{i=1}^n \left[\mathrm{sig}\left(\boldsymbol{s}_i\right)^{\frac{r}{q}}\right]^T \boldsymbol{J}_i\dot{\boldsymbol{s}}_i = \sum_{i=1}^n \left[\mathrm{sig}\left(\boldsymbol{s}_i\right)^{\frac{r}{q}}\right]^T \left(\boldsymbol{J}_i\dot{\boldsymbol{\omega}}_{ei} + \boldsymbol{J}_i\boldsymbol{Q}_i + \Delta\boldsymbol{Q}_i\right) \tag{31}$$

Substituting the relative dynamics Equations (28) into (31) yields

$$\begin{aligned} \dot{V} &= \sum_{i=1}^n \left[\mathrm{sig}\left(\boldsymbol{s}_i\right)^{\frac{r}{q}}\right]^T \left(\boldsymbol{W}_i + \boldsymbol{u}_i + \boldsymbol{d}_i + \Delta\boldsymbol{W}_i + \boldsymbol{J}_i\boldsymbol{Q}_i + \Delta\boldsymbol{Q}_i\right) \\ &= \sum_{i=1}^n \left[\mathrm{sig}\left(\boldsymbol{s}_i\right)^{\frac{r}{q}}\right]^T \left(-\gamma_i \mathrm{sig}\left(\boldsymbol{s}_i\right)^{\frac{p}{q}} + \boldsymbol{d}_i + \Delta\boldsymbol{W}_i + \Delta\boldsymbol{Q}_i + \boldsymbol{u}_{if}\right) \end{aligned} \tag{32}$$

which can be restated in the following form:

$$\dot{V} = \sum_{i=1}^{n} \left[\mathrm{sig}\,(\boldsymbol{s}_i)^{\frac{r}{q}}\right]^T \Big(- \Big[\gamma_i \boldsymbol{I} - \mathrm{diag}(\boldsymbol{d}_i + \Delta\boldsymbol{W}_i + \Delta\boldsymbol{Q}_i)\ \mathrm{diag}^{-1}\left(\mathrm{sig}\,(\boldsymbol{s}_i)^{\frac{p}{q}}\right)\Big] \mathrm{sig}\,(\boldsymbol{s}_i)^{\frac{p}{q}} + \boldsymbol{u}_{if}\Big) \tag{33}$$

For (33), a structure similar to (15) can be obtained if the matrix $\Big[\gamma_i \boldsymbol{I} - \mathrm{diag}(\boldsymbol{d}_i + \Delta\boldsymbol{W}_i + \Delta\boldsymbol{Q}_i)\mathrm{diag}^{-1}\left(\mathrm{sig}(\boldsymbol{s}_i)^{\frac{p}{q}}\right)\Big]$ can be kept positive definite; therefore, finite-time convergence can be guaranteed according to an analysis similar to Theorem 3.1. We use $\hat{\boldsymbol{d}}_i \in R^3$ to represent the matrix $(\boldsymbol{d}_i + \Delta\boldsymbol{W}_i + \Delta\boldsymbol{Q}_i)$ such that

$$(\boldsymbol{d}_i + \Delta\boldsymbol{W}_i + \Delta\boldsymbol{Q}_i) = \hat{\boldsymbol{d}}_i = \begin{bmatrix} \hat{\boldsymbol{d}}_{i(1)} & \hat{\boldsymbol{d}}_{i(2)} & \hat{\boldsymbol{d}}_{i(3)} \end{bmatrix}^T \tag{34}$$

If

$$\gamma_i - \frac{\hat{\boldsymbol{d}}_{i(k)}}{\boldsymbol{s}_{i(k)}} > 0 \text{ for } k = 1, 2, 3, \tag{35}$$

then the region

$$\left|\boldsymbol{s}_{i(k)}^{\frac{p}{q}}\right| \le \frac{\left|\hat{\boldsymbol{d}}_{i(k)}\right|}{\gamma_i} \qquad \|\boldsymbol{s}_i\| \le \left(\frac{\tilde{\Phi}_i}{\gamma_i}\right)^{\frac{q}{p}} \tag{36}$$

can be reached in finite time.

Once the system states reach the region, we have

$$\boldsymbol{s}_i = \hat{\Phi}_i \tag{37}$$

where $\left|\hat{\Phi}_i\right| \le \Phi_i$. Equation (37) can be rewritten as

$$\boldsymbol{\omega}_{ei(k)} + a\boldsymbol{\sigma}_{ei(k)} + b\mathrm{sig}\,(\boldsymbol{\sigma}_{ei})_{(k)}^{\frac{p}{q}} = \hat{\Phi}_i \tag{38}$$

Then, the following two equations can be obtained

$$\begin{aligned} &\boldsymbol{\omega}_{ei(k)} + \left[a - \frac{\hat{\Phi}_i}{\boldsymbol{\sigma}_{ei(k)}}\right]\boldsymbol{\sigma}_{ei(k)} + b\mathrm{sig}\,(\boldsymbol{\sigma}_{ei})_{(k)}^{\frac{p}{q}} = 0 \\ &\boldsymbol{\omega}_{ei(k)} + a\boldsymbol{\sigma}_{ei(k)} + \left[b - \frac{\hat{\Phi}_i}{\mathrm{sig}\,(\boldsymbol{\sigma}_{ei})_{(k)}^{\frac{p}{q}}}\right]\mathrm{sig}\,(\boldsymbol{\sigma}_{ei})_{(k)}^{\frac{p}{q}} = 0 \end{aligned} \tag{39}$$

Equation (39) will still keep the same structure with the sliding surface $\boldsymbol{s}_i$ if

$$\left|\boldsymbol{\sigma}_{ei(k)}\right| > \min\left[\frac{\left|\hat{\Phi}_i\right|}{a}, \left(\frac{\left|\hat{\Phi}_i\right|}{b}\right)^{\frac{q}{p}}\right] \tag{40}$$

Therefore, the attitude tracking error of the ith spacecraft will reach the following region

$$\left|\boldsymbol{\sigma}_{ei(k)}\right| \le \min\left[\frac{\left|\hat{\Phi}_i\right|}{a}, \left(\frac{\left|\hat{\Phi}_i\right|}{b}\right)^{\frac{q}{p}}\right] \le \min\left[\frac{\Phi_i}{a}, \left(\frac{\Phi_i}{b}\right)^{\frac{q}{p}}\right] \tag{41}$$

in finite time. Hence, the proof is completed.

Besides being sufficiently smooth and its derivative being bounded, no other constraints have been imposed on the desired trajectory, and the angular velocity of the spacecraft is

not required to be non-null in the theoretical analysis. Consequently, the desired trajectory could be "arbitrary" which means that it does not need to be a dynamic one but also a static one. In this sense, the proposed control schemes also solve the attitude regulation problem for a spacecraft formation.

Since there is no assumption on the parameter δ_{ij}, the effectiveness of the proposed synchronization control laws is not affected by the type of the communication topology. Besides the undirected graph considered in [4-8,11-15], the topology can also be directed, full-connected or connected, static or even dynamic when δ_{ij} switches between 0 and 1 during the flying mission. By virtue of this, the proposed control schemes are competent under arbitrary communication topologies, and the reliability of the formation is improved since the stability and convergence of the formation system can still be guaranteed when communication failures occur. Nevertheless, it should be noted that the control performance will descend in the face of a disconnected communication topology since the formation keeping control action, which is used to improve the performance of the formation control, will be deactivated by the disconnected topology.

The traditional TSM control laws [21-24] have to be discontinuous to guarantee the finite-time convergent property. Such discontinuity will cause chattering phenomenon which, as well-known, is harmful for any mechanical system since it involves extremely high control activity and may excite high-frequency dynamics neglected in the course of modeling. Therefore, it should be eliminated for the controller to perform properly. As an approximation to the discontinuous function used in traditional TSM control laws, the boundary-layer approach [29] using sigmoid functions is able to alleviate the chattering. However, it can only guarantee finite-time convergence to the boundary layer. Inside the boundary layer, only asymptotic convergence can be achieved. On the other hand, we developed a class of continuous finite-time control laws herein without using the approximation method. The proposed control laws are continuous and so are chattering-free. Moreover, the finite-time reachability to the equilibrium can be guaranteed simultaneously.

It is not surprising that the performance of the system, especially the robustness, highly depends on the control parameters γ_i, a and b. From the previous analysis it can be seen that the neighborhood Φ_i is a result of the terminal sliding mode control with fractional power $\frac{p}{q}$. If the parameter γ_i are chosen large enough so that

$$\gamma_i > \tilde{\Phi}_i, \tag{42}$$

then $\Phi_i < 1$. Because $\frac{q}{p} > 1$, the exponential term $\frac{q}{p}$ in Φ_i will greatly reduce the size of Φ_i. Similarly, the size of the region (40) can be reduced by chosen parameters a and b properly such that $a, b > \hat{\Phi}_i$. Therefore, if large control parameters are available, the developed control laws (10) may lead to respectable tracking performance in the presence of poor dynamic models and large disturbing torques.

The tuning of the control parameters γ_i, a and b in practice is typically done experimentally, and their values are limited by the frequency of the lowest unmodeled structural resonant mode, the largest time-delay in actuators and the sampling rate in practical situation [29]. Furthermore, there is a trade-off between control accuracy and settling time: high control accuracy can be obtained by large control parameters but at a cost of long settling time. Hence, the value of the control parameters γ_i, a and b should be chosen according to the system's mechanical properties, the limitations on the actuators and the available computing power.

Since the sign function in the control laws will cause chattering in the control signal that should be avoided, the saturation function below (or any other sigmoid function) can

be utilized to replace the sign function:

$$\mathrm{sat}(x) = \begin{cases} 1 & x > \mu \\ x/\mu & |x| \le \mu \\ -1 & x < -\mu \end{cases} \tag{43}$$

where μ is small positive constant.

4. **Numerical Simulations.** In this section, numerical simulations of a low-earth-orbit (LEO) formation composed of four spacecraft are provided to validate the stability characteristics of the proposed control schemes. A formation flying mission where the four spacecraft are required to align their attitudes while tracking the attitude of another spacecraft defined by [30] $\boldsymbol{\omega}_d = \begin{pmatrix} -0.01 & 0.01 & 0.01 \end{pmatrix}^T$ rad/s and $\boldsymbol{\sigma}_d(0) = \begin{pmatrix} 0.1 & 0.3 & 0.2 \end{pmatrix}^T$ is considered. The simulations will be done in two scenarios. The first scenario will test the effectiveness of the proposed control schemes in the presence of large initial attitude errors, external disturbances, parameter uncertainties, communication delays and dynamic communication topologies. The second scenario will analyze the effects of the control parameters on control performance.

The nominal inertia tensor of each spacecraft is chosen as

$$\boldsymbol{J}_1 = \begin{pmatrix} 20 & 0 & 2 \\ 0 & 25 & 0 \\ 2 & 0 & 29 \end{pmatrix} \mathrm{kg \cdot m^2}, \quad \boldsymbol{J}_2 = \begin{pmatrix} 22 & 1 & 0.5 \\ 1 & 24 & 3 \\ 0.5 & 3 & 22 \end{pmatrix} \mathrm{kg \cdot m^2},$$

$$\boldsymbol{J}_3 = \begin{pmatrix} 25 & 0.8 & 2 \\ 0.8 & 29 & 1 \\ 2 & 1 & 21 \end{pmatrix} \mathrm{kg \cdot m^2}, \quad \boldsymbol{J}_4 = \begin{pmatrix} 23 & 0.4 & 0 \\ 0.4 & 26 & 0.8 \\ 0 & 0.8 & 28 \end{pmatrix} \mathrm{kg \cdot m^2}$$

with the perturbation inertia tensor $\Delta \boldsymbol{J}_i = 0.3 \boldsymbol{J}_i$.

The initial attitude states of the spacecraft formation are chosen as follows:

$$\boldsymbol{\omega}_1(0) = \begin{pmatrix} 0.045 & -0.043 & 0.077 \end{pmatrix}^T \mathrm{rad/s}, \quad \boldsymbol{\sigma}_1(0) = \begin{pmatrix} 0.2 & 0.2 & -0.2 \end{pmatrix}^T;$$

$$\boldsymbol{\omega}_2(0) = \begin{pmatrix} 0.052 & -0.026 & 0.033 \end{pmatrix}^T \mathrm{rad/s}, \quad \boldsymbol{\sigma}_2(0) = \begin{pmatrix} 0.3 & 0.2 & 0.3 \end{pmatrix}^T;$$

$$\boldsymbol{\omega}_3(0) = \begin{pmatrix} -0.026 & 0.022 & -0.013 \end{pmatrix}^T \mathrm{rad/s}, \quad \boldsymbol{\sigma}_3(0) = \begin{pmatrix} -0.2 & 0.1 & -0.1 \end{pmatrix}^T;$$

$$\boldsymbol{\omega}_4(0) = \begin{pmatrix} -0.037 & -0.019 & 0.023 \end{pmatrix}^T \mathrm{rad/s}, \quad \boldsymbol{\sigma}_4(0) = \begin{pmatrix} 0.4 & -0.2 & 0.1 \end{pmatrix}^T.$$

A spacecraft formation in LEO is mainly affected by the gravity gradient torque, while the disturbances such as the solar radiation pressure torque will be dominant for a formation in high-earth orbits such as the geostationary orbit. All these torques are slowly varying and can be treated as signals composed of constants and periodic trigonometric functions. Taking account of these factors, the disturbances are chosen as

$$\boldsymbol{u}_{di} = \boldsymbol{u}_{li} + \boldsymbol{u}_{uni}$$

where

$$\boldsymbol{u}_{l1} = \begin{pmatrix} 0.0012 & -0.0018 & 0.0012 \end{pmatrix}^T \mathrm{N \cdot m}, \ \boldsymbol{u}_{l2} = \begin{pmatrix} 0.001 & 0.0014 & -0.0017 \end{pmatrix}^T \mathrm{N \cdot m},$$

$$\boldsymbol{u}_{l3} = \begin{pmatrix} -0.0013 & 0.0016 & -0.001 \end{pmatrix}^T \mathrm{N \cdot m}, \ \boldsymbol{u}_{l4} = \begin{pmatrix} 0.0015 & -0.0014 & -0.0013 \end{pmatrix}^T \mathrm{N \cdot m}$$

denote the constant disturbing torques and

$$\boldsymbol{u}_{uni} = \frac{1}{5} \begin{pmatrix} u_{li(1)} \sin\left(\frac{t}{12}\right) \\ u_{li(2)} \cos\left(\frac{t}{15}\right) \\ u_{li(3)} \sin\left(\frac{t}{10}\right) \cos\left(\frac{t}{15}\right) \end{pmatrix}$$

is used to simulate the unmodelled disturbances and similar effects.

The parameter δ_{ij} is given by

$$\delta_{12}(t) = \begin{cases} 1 & \text{for mod } (t, 10) \leq 6 \\ 0 & \text{for mod } (t, 10) > 6 \end{cases}$$

$$\begin{aligned} \delta_{12}(t) &= \delta_{13}(t+1) = \delta_{14}(t+1.3) = \delta_{21}(t+3.2) = \delta_{23}(t+0.3) = \delta_{24}(t+0.2) \\ &= \delta_{31}(t+4) = \delta_{32}(t+2.4) = \delta_{34}(t+4.6) = \delta_{41}(t+3) \\ &= \delta_{42}(t+1.9) = \delta_{43}(t+0.8) \end{aligned}$$

to describe a time-varying communication topology, where $\text{mod}(x, y)$ represents the remainder of dividing x by y.

The control torque is bounded as $\left|\boldsymbol{u}_{i(k)}\right| \leq 0.2$ N·m. The control parameters are chosen as $\gamma_i = 0.5$, $k_i = 0.4$, $a = 0.3$, $b = 0.5$, $p = 5$, $r = 7$ and $q = 9$. Control performance of the formation is measured by an absolute error metric and a relative error metric.

The proposed controller is compared with the controller in [31] to demonstrate its advantages and evaluate its performance. An attitude coordinated adaptive control law

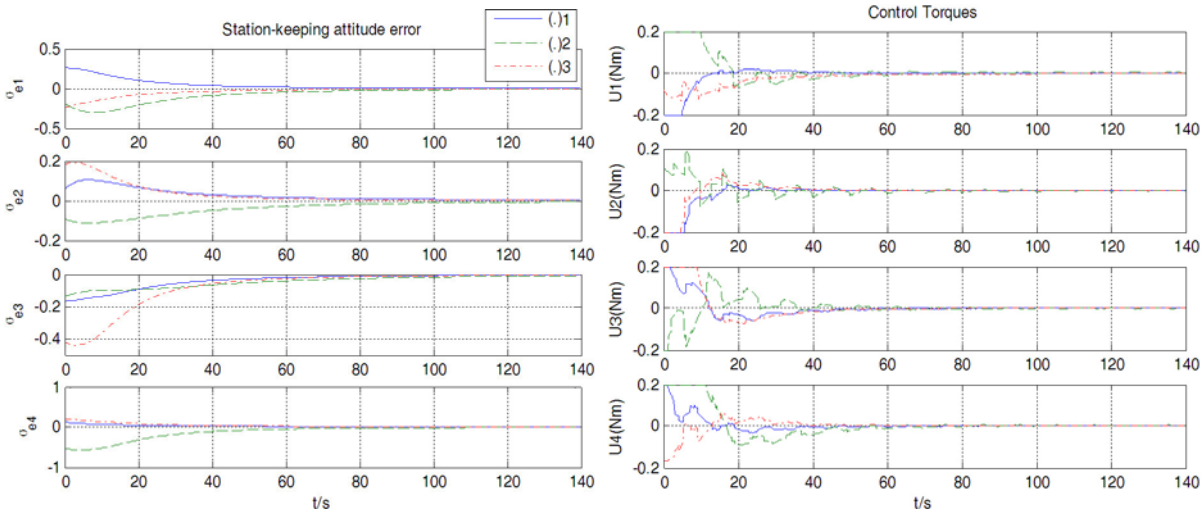

(a) Absolute attitude errors

(b) Control Torques

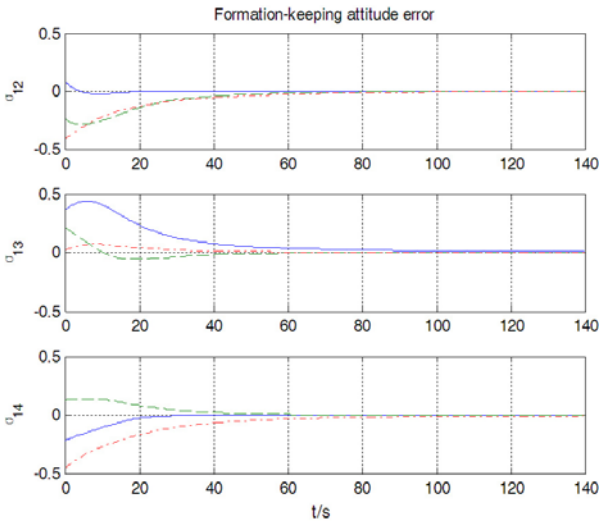

(c) Relative attitude errors

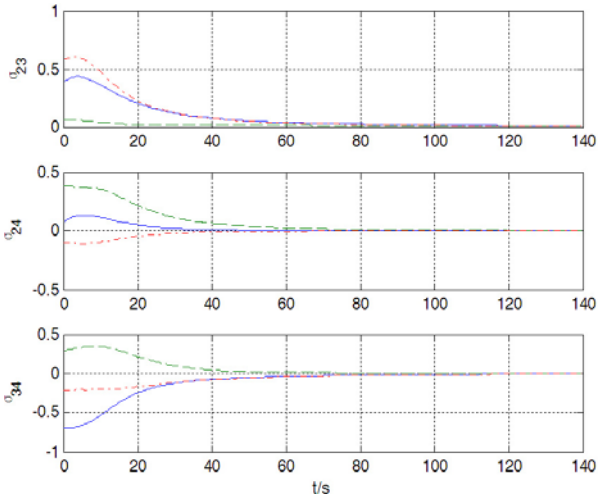

(d) Relative attitude errors

FIGURE 1. Evolutions of the attitude errors of the proposed controller

for the latter is designed and written as

$$\boldsymbol{u}_i = -\boldsymbol{G}_i^T(\boldsymbol{\sigma}_{ei}) K_{p_i}\boldsymbol{\sigma}_{ei} - K_{d_i}\boldsymbol{\omega}_{ei} - \rho_i sign(\boldsymbol{s}_i) \tag{44}$$

where $\boldsymbol{s}_i = \boldsymbol{\omega}_{ei} + c\frac{\boldsymbol{\sigma}_{ei}}{1+\boldsymbol{\sigma}_{ei}^T\boldsymbol{\sigma}_{ei}}$, K_{p_i}, K_{d_i} are positive definite matrices.

The parameters of the controller respectively are

$$K_{pi} = \begin{bmatrix} 20 & 0 & 0 \\ 0 & 20 & 0 \\ 0 & 0 & 20 \end{bmatrix}, \quad K_{di} = \begin{bmatrix} 300 & 0 & 0 \\ 0 & 300 & 0 \\ 0 & 0 & 300 \end{bmatrix}, \quad \rho_i = 1, \quad c_i = 0.6$$

4.1. **Numerical validation of the theoretical analysis.** The simulation in this subsection is to validate the theoretical analysis in the previous section. Simulation results are presented in Figure 1. In (a), (c) and (d), the absolute attitude error and the relative attitude error are shown, respectively. (b) illustrates the control torques applied on each spacecraft.

The theoretical analysis of the proposed control schemes is validated by the simulations. From the plots in (a), (c) and (d) it can be seen that synchronization is realized in the

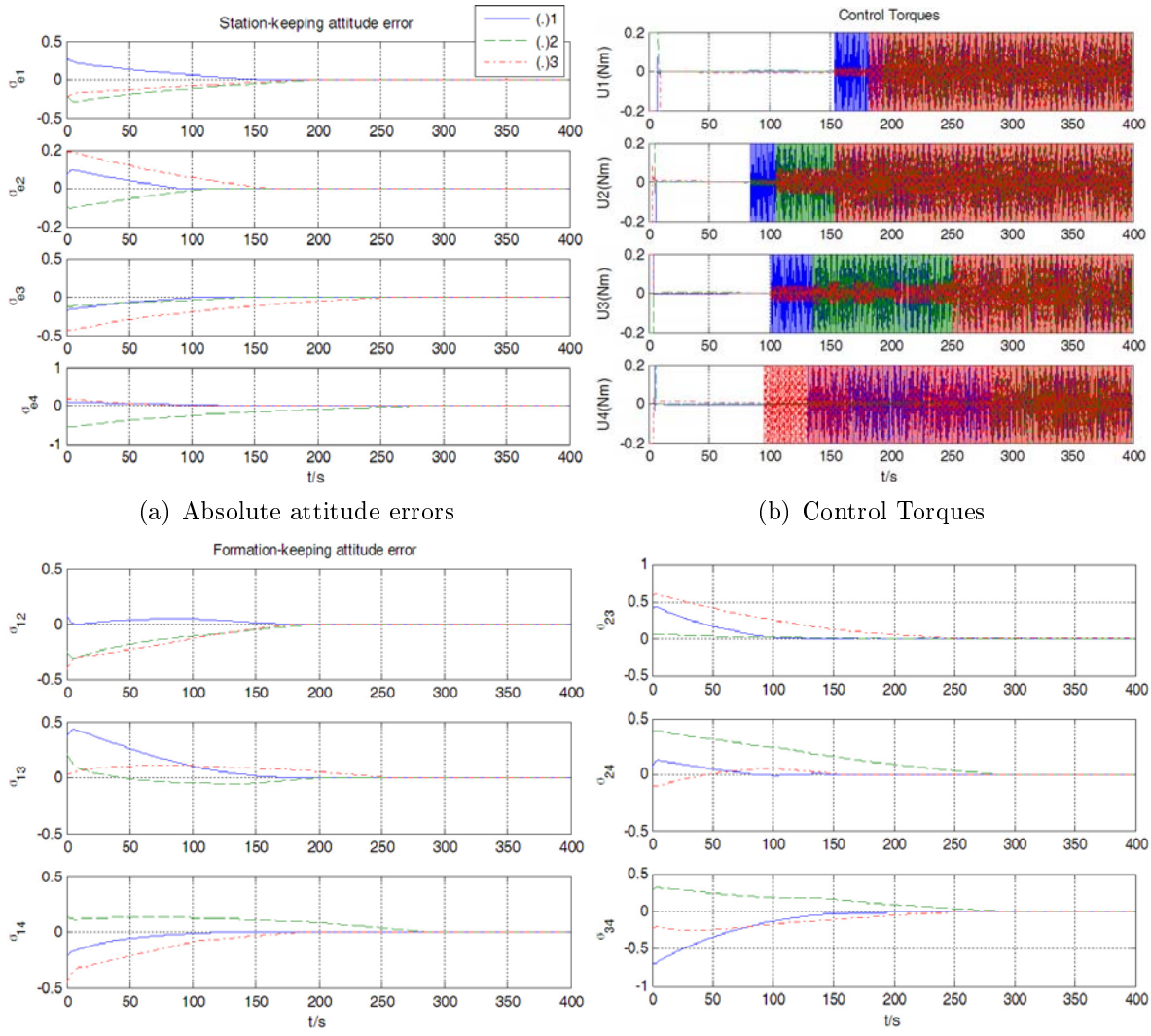

(a) Absolute attitude errors

(b) Control Torques

(c) Relative attitude errors

(d) Relative attitude errors

FIGURE 2. Evolutions of the attitude errors of the controller (38)

presence of communication delays, parameter uncertainties, disturbances, and a time-varying topology. Settling time of both AE and RE is 110 sec approximately. The final absolute attitude angular velocity errors are better than -4.543×10^{-4} rad/s, and relative attitude angular velocity errors are better than 5.323×10^{-4} rad/s. In (b), bounded control torques are demonstrated.

Figure 2 shows the simulation results of the closed-loop system with controller (38). The setting time of AE is 250s and the setting time of RE is 300s. And the sign function causes chattering. The final absolute attitude angular velocity error are better than -7.327×10^{-4} rad/s, and relative attitude angular velocity errors are better than 0.0015 rad/s. In (b), bounded control torques are demonstrated. Compared with the controller (38), the proposed controller provides the rapid convergence and achieves high tracking accuracy.

4.2. **Control parameters analysis.** In order to make meaningful comparisons, investigating the effects of various control parameters on control performances requires that the other parameters are held constant. In this subsection, three scenarios are considered, and the investigation is implemented by varying different control parameters while holding the other parameters constant.

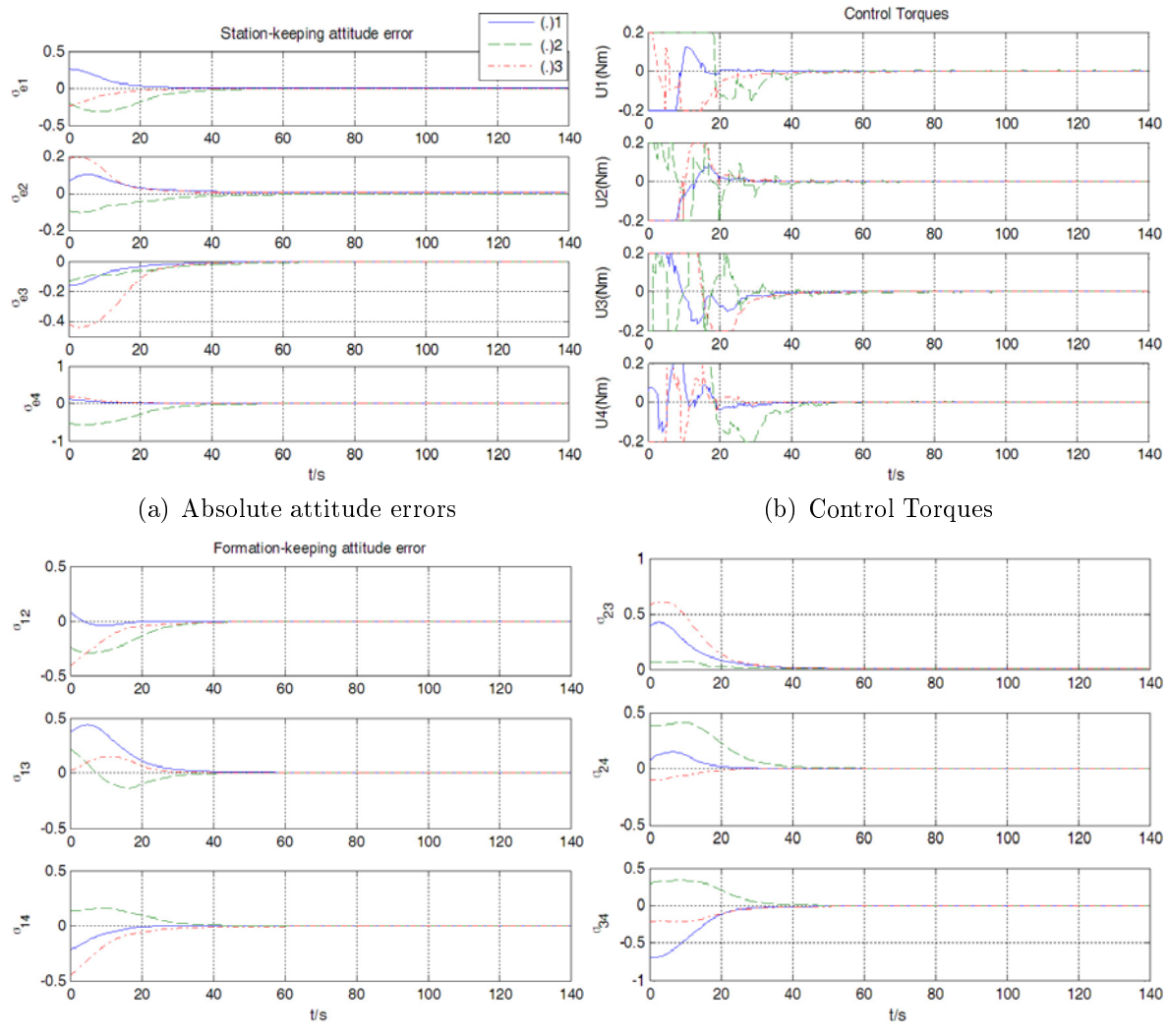

(a) Absolute attitude errors

(b) Control Torques

(c) Relative attitude errors

(d) Relative attitude errors

FIGURE 3. Evolutions of the attitude errors of Case A

Case A: By doubling the control parameters γ_i, a, and b as $\gamma_i = 1$, $a = 0.6$, and $b = 1$, simulation results are presented in Figure 3.

Figure 3(a) illustrates the absolute attitude error metric, and (c) and (d) show the relative attitude error metric. From the result it can be seen that the absolute attitude angular velocity errors are better than -6.658×10^{-5} and relative attitude angular velocity errors are better than 8.056×10^{-5}, which are improved significantly compared with Figure 1. Nevertheless, settling time also decreases to 60 sec due to the larger control parameters. The results validate the discussion on control parameters in the previous section: large control parameters γ_i, a, and b could result in high control accuracy and at a cost of short settling time, but meanwhile it will cause large chattering.

Case B: Effect of the formation keeping control action on control performance is demonstrated in Figure 4 by choosing $k_i = 0$. Absolute attitude error metric and relative attitude error metric are shown in (a), (c) and (d), respectively. As shown in Figure 4, both the settling time and the attitude control error increase significantly: settling time of AE and RE increases to 160 sec, the largest final absolute attitude angular velocity error is 4.967×10^{-4}rad/s, and relative attitude angular velocity error is 5.663×10^{-4}rad/s.

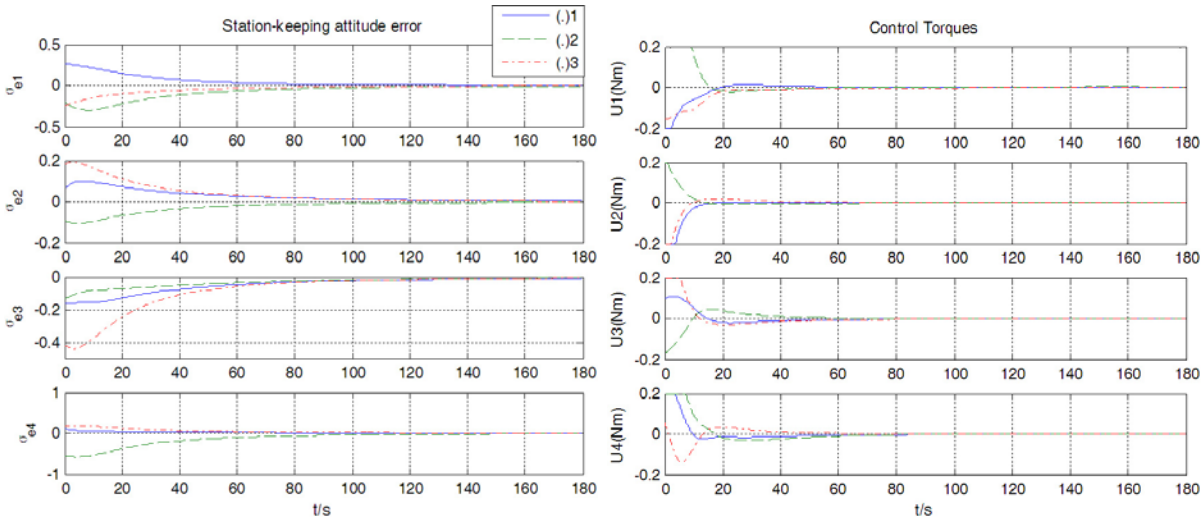

(a) Absolute attitude errors

(b) Control Torques

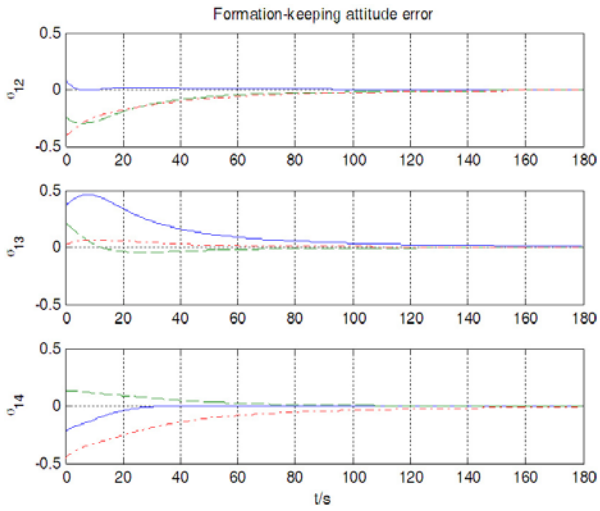

(c) Relative attitude errors

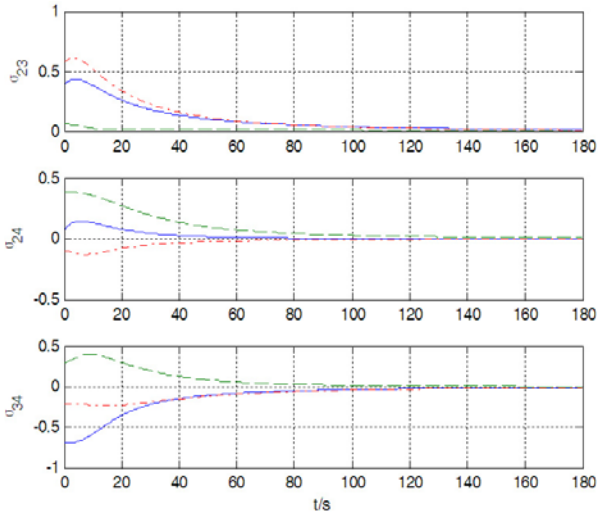

(d) Relative attitude errors

FIGURE 4. Evolutions of the attitude errors of Case B

Compared with Figure 1, the effect of formation keeping control action is illustrated. The increased steady-state values and settling time demonstrate that albeit finite-time convergence can still be guaranteed with no formation keeping control term, performance of the formation is affected since the formation keeping term is used to enforce the interconnection between the spacecraft within the formation, and thus improves the performance of the formation system. Therefore, the formation keeping control term is critical for a satisfactory performance of the formation.

Case C: Results in Figure 5 demonstrate the control performance with various connection weights. By varying the connection weight $k_i = 0.8$, absolute attitude error metric and relative attitude error metric are illustrated in (a), (b) and (c), respectively. Compared with Figure 1 and Figure 4, these weights are able to guarantee finite-time convergence of the formation system. Nevertheless, control performances are various according to different weights. The steady-state value of RE decreases with increasing connection weight, but AE is not affected. Therefore, an improvement in relative control performance can be achieved by enlarging connection weights.

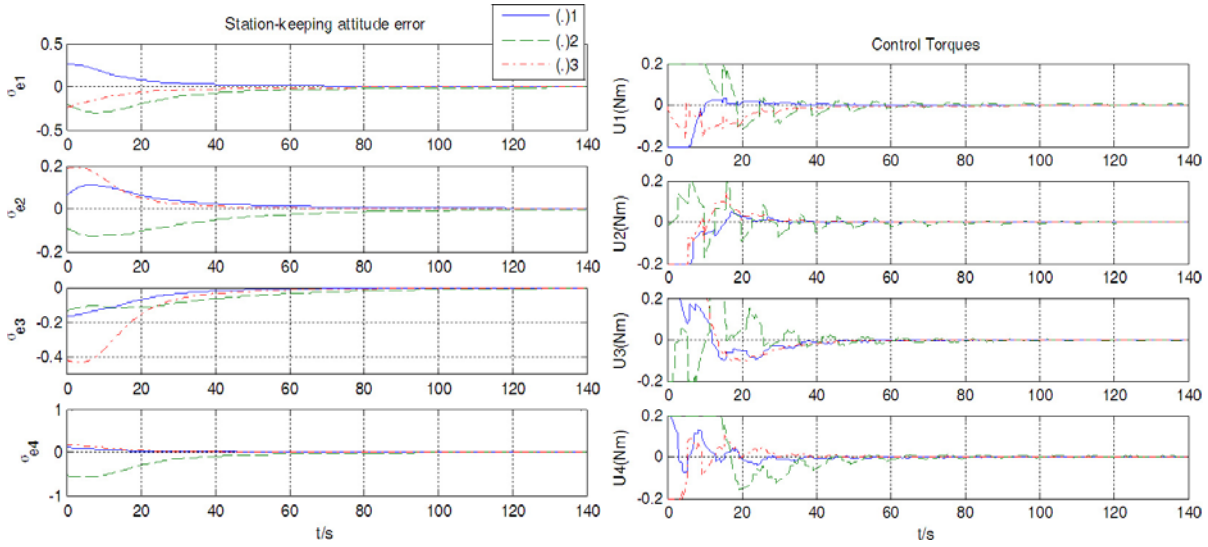

(a) Absolute attitude errors

(b) Control Torques

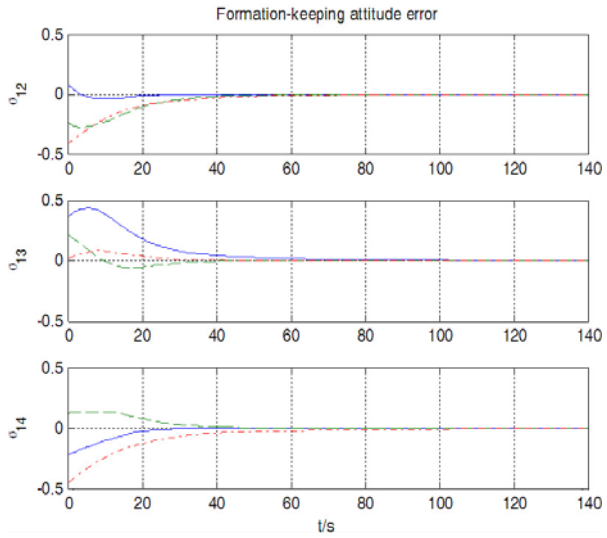

(c) Relative attitude errors

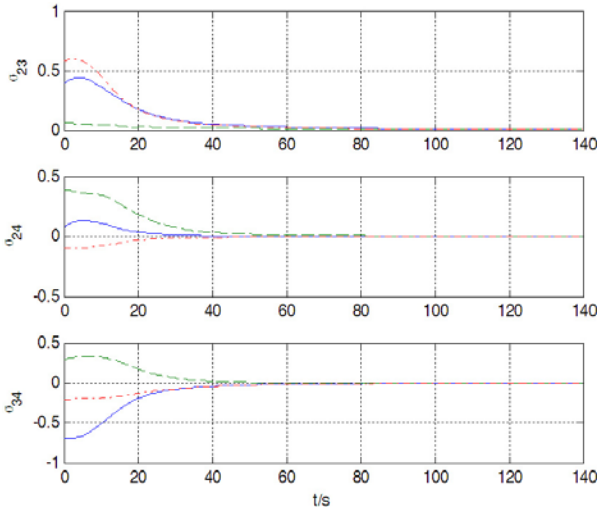

(d) Relative attitude errors

FIGURE 5. Evolutions of the attitude errors of Case C

5. **Conclusion.** In this paper, a continuous attitude control approach with finite-time convergent property is proposed for attitude synchronization of spacecraft formations. The proposed continuous control schemes could guarantee finite-time reachability of desired trajectory subject to communication delays. High control precision, chattering attenuation, and robustness were achieved simultaneously by choosing the control parameters properly. Simulations of a four-spacecraft formation in the presence of communication delays, parameter uncertainties, external disturbances and dynamic communication graphs validated the theoretical analysis. By varying control parameters, control performances of the formation were also analyzed through simulations. Simulation results demonstrated the effects of control parameters on formation performance and the indispensability of formation keeping control term. They also showed that increasing the connection weights decreased the relative attitude control errors.

Acknowledgment. Research for this paper is supported by the National Natural Science Foundation of China, grant 60704020. The authors express their sincere gratitude to Prof. Marco Lovera of Politecnico di Milano for English writing and constructive comments.

REFERENCES

[1] P. K. C. Wang and F. Y. Hadaegh, Coordination and control of multiple microspacecraft moving in formation, *Journal of the Astronautical Sciences*, vol.44, no.3, pp.315-355, 1996.

[2] J. Lawton and R. W. Beard, Synchronized multiple spacecraft rotations, *Automatica*, vol.38, no.8, pp.1359-1364, 2002.

[3] P. K. C. Wang, F. Y. Hadaegh and K. Lau, Synchronized formation rotation and attitude control of multiple free-flying spacecraft, *Journal of Guidance, Control and Dynamics*, vol.22, no.1, pp.28-35, 1999.

[4] I. Chang, S. Park and K. Choi, Decentralized coordinated attitude control for satellite formation flying via the state-dependent Riccati equation technique, *International Journal of Non-Linear Mechanics*, vol.44, no.8, pp.891-904, 2009.

[5] W. Ren and R. W. Beard, Decentralized scheme for spacecraft formation flying via the virtual structure approach, *Journal of Guidance, Control and Dynamics*, vol.27, no.1, pp.73-82, 2004.

[6] M. C. VanDyke and C. D. Hall, Decentralized coordinated attitude control within a formation of spacecraft, *Journal of Guidance, Control and Dynamics*, vol.29, no.5, pp.1101-1109, 2006.

[7] H. Liang, J. Wang and Z. Sun, Robust decentralized coordinated attitude control of spacecraft formation, *Acta Astronautica*, vol.69, nos.5-6, pp.280-288, 2011.

[8] E. Jin, X. Jiang and Z. Sun, Robust decentralized attitude coordination control of spacecraft formation, *Systems & Control Letters*, vol.57, no.7, pp.567-577, 2008.

[9] A. Sarlette, R. Sepulchre and N. E. Leonard, Autonomous rigid body attitude synchronization, *Automatica*, vol.45, no.2, pp.572-577, 2009.

[10] B. Wu and D. Wang, Decentralized robust adaptive control for attitude synchronization under directed communication topology, *Journal of Guidance, Control and Dynamics*, vol.3, no.4, pp.1276-1282, 2011.

[11] E. Jin and Z. Sun, Robust attitude synchronization controllers design for spacecraft formation, *IET Control Theory & Applications*, vol.3, no.3, pp.325-339, 2009.

[12] Z. Meng, W. Ren and Z. You, Distributed finite-time attitude containment control for multiple rigid bodies, *Automatica*, vol.46, no.12, pp.2092-2099, 2010.

[13] H. Bai, M. Arcak and J. T. Y. Wen, Rigid body attitude coordination without inertial frame information, *Automatica*, vol.44, no.12, pp.3170-3175, 2008.

[14] D. V. Dimarogonas, P. Tsiotras and K. J. Kyriakopoulos, Leader-follower cooperative attitude control of multiple rigid bodies, *Systems & Control Letters*, vol.58, no.6, pp.429-435, 2009.

[15] Z. Meng, W. Ren and Z. You, Decentralised cooperative attitude tracking using modified Rodriguez parameters based on relative attitude information, *International Journal of Control*, vol.83, no.12, pp.2427-2439, 2010.

[16] S. Liu, L. Xie and H. Zhang, Distributed consensus for multi-agent systems with delays and noises in transmission channels, *Automatica*, vol.47, pp.920-934, 2011.

[17] J. Yu and L. Wang, Group consensus in multi-agent systems with switching topologies and communication delays, *Systems & Control Letters*, vol.59, pp.340-348, 2010.
[18] J. Qin, H. Gao and W. Zheng, Second-order consensus for multi-agent systems with switching topology and communication delay, *Systems & Control Letters*, vol.60, pp.390-397, 2011.
[19] N. Chopra, M. W. Spong and R. Lozano, Synchronization of bilateral teleoperators with time delay, *Automatica*, vol.44, no.8, pp.2142-2148, 2008.
[20] S. J. Chung, U. Ahsun and J. J. E. Slotine, Application of synchronization to formation flying spacecraft: Lagrangian approach, *Journal of Guidance, Control, and Dynamics*, vol.32, no.2, pp.512-526, 2009.
[21] Y. Hong, J. Wang and D. Cheng, Adaptive finite-time control of nonlinear systems with parametric uncertainty, *IEEE Trans. Automatic Control*, vol.51, no.5, pp.858-862, 2006.
[22] Y. Hong, Y. Xu and J. Huang, Finite-time control for robot manipulators, *Systems & Control Letters*, vol.46, no.4, pp.243-253, 2002.
[23] L. T. Gruyitch and A. Kokosy, Robot control for robust stability with finite reachability time in the whole, *Journal of Robotic Systems*, vol.16, no.5, pp.263-283, 1999.
[24] T. Li and Y. Huang, MIMO adaptive fuzzy terminal sliding-mode controller for robotic manipulators, *Information Sciences*, vol.180, no.23, pp.4641-4660, 2010.
[25] S. Yu, X. Yu, B. Shirinzadeh and Z. Man, Continuous finite-time control for robotic manipulators with terminal sliding mode, *Automatica*, vol.41, no.11, pp.1957-1964, 2005.
[26] L. Yang and J. Yang, Robust finite-time convergence of chaotic systems via adaptive terminal sliding mode scheme, *Communications in Nonlinear Science and Numerical Simulation*, vol.16, no.6, pp.2405-2413, 2011.
[27] H. Schaub and J. L. Junkins, *Analytical Mechanics of Space Systems*, AIAA Educational Series, AIAA, Reston, VA, 2003.
[28] Y. Hong, H. O. Wang and L. G. Bushnell, Adaptive finite-time control of nonlinear systems, *Proc. of the American Control Conference*, vol.6, pp.4149-4154, 2001.
[29] J. E. Slotine and W. P. Li, *Applied Nonlinear Control*, Prentice Hall, NJ, USA, 1991.
[30] W. Ren and R. W. Beard, Formation feedback control for multiple spacecraft via virtual structures, *IEEE Proceedings: Control Theory and Applications*, vol.151, no.3, pp.357-368, 2004.
[31] E. Jin and Z. Sun, Robust attitude tracking control of flexible spacecraft for achieving globally asymptotic stability, *Int. J. of Robust and Nonlinear Control*, vol.19, pp.1201-1223, 2009.